Available online at www.sciencedirect.com
SCIENCE DIRECT®
Solid State Ionics 160 (2003) 247–258
SOLID STATE IONICS
www.elsevier.com/locate/ssi

Oxygen transport in $Ce_{0.8}Gd_{0.2}O_{2-\delta}$-based composite membranes

V.V. Kharton[a,b,*], A.V. Kovalevsky[b], A.P. Viskup[b], A.L. Shaula[a], F.M. Figueiredo[a], E.N. Naumovich[b], F.M.B. Marques[a]

[a] *Department of Ceramics and Glass Engineering, CICECO, University of Aveiro, 3810-193 Aveiro, Portugal*
[b] *Institute of Physicochemical Problems, Belarus State University, 14 Leningradskaya Str., 220050 Minsk, Belarus*

Received 8 August 2001; received in revised form 9 April 2003; accepted 10 April 2003

Abstract

Gadolinia-doped ceria electrolyte $Ce_{0.8}Gd_{0.2}O_{2-\delta}$ (CGO) and perovskite-type mixed conductor $La_{0.8}Sr_{0.2}Fe_{0.8}Co_{0.2}O_{3-\delta}$ (LSFC), having compatible thermal expansion coefficients (TECs), were combined in dual-phase ceramic membranes for oxygen separation. Oxygen permeability of both LSFC and composite LSFC/CGO membranes at 970–1220 K was found to be limited by the bulk ambipolar conductivity. LSFC exhibits a relatively low ionic conductivity and high activation energy for ionic transport (~ 200 kJ/mol) in comparison with doped ceria. As a result, oxygen permeation through LSFC/CGO composite membranes, containing similar volume fractions of the phases, is determined by the ionic transport in CGO. The permeation fluxes through LSFC/CGO and $La_{0.7}Sr_{0.3}MnO_{3-\delta}/Ce_{0.8}Gd_{0.2}O_{2-\delta}$ (LSM/CGO) composites have comparable values. An increase in the p-type electronic conductivity of ceria in oxidizing conditions, which can be achieved by co-doping with variable-valence metal cations, such as Pr, leads to a greater permeability. The oxygen ionic conductivity of the composites consisting of CGO and perovskite oxides depends strongly of processing conditions, decreasing with interdiffusion of the phase components, particularly lanthanum and strontium cations from the perovskite into the CGO phase.

Keywords: Composite; Ceria; Perovskite; Membrane; Oxygen permeation

1. Introduction

Dense mixed-conducting ceramic membranes are of significant interest due to their potential applications for high-purity oxygen separation, partial oxidation of hydrocarbons, and sensors [1–8]. The main advantages of such membranes include an infinite theoretical permselectivity with respect to oxygen, and an ability to integrate oxygen separation, steam reforming and partial oxidation into one single step for the natural gas conversion. This may provide considerable economical benefits because the most significant cost associated with the synthesis-gas generation by the methane oxidation is that of an oxygen plant. At the same time, the application of the ceramic membranes is essentially limited by numerous specific disadvantages of the mixed-conducting membrane materials known at the present time. In particular, perovskite-related phases $(A,Ln)(Co,Fe)O_{3-\delta}$ (A = Sr, Ba; Ln is the rare-earth element) having the

* Corresponding author. Present address: Department of Ceramics and Glass Engineering, UIMC, University of Aveiro, 3810-193 Aveiro, Portugal. Tel.: +351-234-370263; fax: +351-234-425300.
E-mail address: kharton@cv.ua.pt (V.V. Kharton).

0167-2738/03/$ - see front matter © 2003 Elsevier Science B.V. All rights reserved.
doi:10.1016/S0167-2738(03)00183-8

highest oxygen permeability in oxidizing conditions are thermodynamically and/or dimensionally unstable under large oxygen chemical potential gradients such as "air/methane" [1,4,9–11]. In addition, the most-permeable perovskite-type oxides exhibit an ordering in the oxygen sublattice and a high reactivity with gas species such as CO_2 at temperatures below 1000–1070 K, leading to degradation in behavior with time [1,9–12].

Another group of membrane materials based on ionic conductors with fluorite- and pyrochlore-type structure, doped with transition metal cations, possesses too low electronic conductivity limiting oxygen transport [1,6,13,14]. The application of such materials is possible in the so-called dual-phase membranes consisting of a mixture of an oxide ionic conductor and an electronically conducting phase [1,2]. A number of oxide solid electrolytes and both metal and oxide electronic conductors have been tested in composite membranes (for example, Refs. [1,2,15,16]). However, the dual-phase membranes show, as a rule, significantly lower permeation fluxes as compared to single-phase mixed conductors. The only exception refers to the composites of stabilized δ-Bi_2O_3 and metallic silver [15,16], which have significant oxygen permeability at 870 to 1100 K but may be unstable due to decomposition of the stabilized δ-Bi_2O_3 phase at temperatures below 900–920 K as well as reactivity of bismuth oxide with silver at T>850 K [17]. Therefore, further developments of the membrane materials are still necessary.

Following our research on CeO_2-based mixed conductors [18–23], the present work is centered on the study of composite membranes consisting of perovskite-type lanthanum–strontium ferrite–cobaltite, $La_{0.8}Sr_{0.2}Fe_{0.8}Co_{0.2}O_{3-\delta}$ (LSFC), and one of the most promising oxide solid electrolytes, gadolinia-doped ceria $Ce_{0.8}Gd_{0.2}O_{2-\delta}$ (CGO20). For comparison, selected data on $La_{0.7}Sr_{0.3}MnO_{3-\delta}$-$Ce_{0.8}Gd_{0.2}O_{2-\delta}$ (LSM/CGO) composites reported in Ref. [18] are also included.

2. Experimental

Dense ceramics of CGO20, LSFC, $Ce_{0.80}Gd_{0.18}Pr_{0.02}O_{2-\delta}$ (CGPO), and LSFC/CGO, LSFC/CGPO and LSM/CGO composites were prepared from commercially available powders (Praxair Specialty Ceramics, Seattle). The sintering conditions of gas-tight samples and list of their abbreviations are given in Table 1. For the LSFC/CGO and LSFC/CGPO composite preparation, the powders of LSFC and CGO20 or CGPO were annealed in air at 1370 K for 6 h, slowly cooled, and then mixed in the 50:50 wt.% proportion by ball-milling for 7–8 h. A similar route described in Ref. [18] was used to prepare LSM/CGO composite. The mixtures were pressed into disk-shaped pellets at 250 to 300 MPa and sintered in air (Table 1).

Estimations of the relative volume fractions of the phases from their weight ratio and theoretical densities, calculated using X-ray diffraction (XRD) data, showed that in the studied LSFC/CGO composites the volume ratio between LSFC and ceria-based phases is approximately 52:48, with an accuracy of 1%. For example, for LSFC/CGO-1 series this ratio was 52.1:47.9. Very similar phase volume ratio was in the LSM/CGO composite used in this work for comparison (52.3:47.7). This ratio should ensure percola-

Table 1
Abbreviations and sintering conditions of the ceramic materials under study

Abbreviation	Composition	Sintering conditions		
		T, K	Time, h	Heating/cooling rate, K/min
CGO20	$Ce_{0.80}Gd_{0.20}O_{2-\delta}$	1873	4	5/10
CGPO	$Ce_{0.80}Gd_{0.18}Pr_{0.02}O_{2-\delta}$	1873	6	5/5
LSFC	$La_{0.8}Sr_{0.2}Fe_{0.8}Co_{0.2}O_{3-\delta}$	1698	2	10/10
LSM	$La_{0.7}Sr_{0.3}MnO_{3-\delta}$	1743	5	5/10
LSFC/CGO-1	Composite of LSFC and CGO20 (50:50 wt.%)	1773	2	10/12
LSFC/CGO-2	Composite of LSFC and CGO20 (50:50 wt.%)	1698–1828[a]	12	10/12
LSFC/CGPO	Composite of LSFC and CGPO (50:50 wt.%)	1773	2	10/12
LSM/CGO	Composite of LSM and CGO20 (50:50 wt.%)	1793	4	5/5

[a] The samples were sintered in the course of increasing temperature from 1698 to 1828 K by steps of 10–20 K. Duration of each temperature step was 1 h.

tion of both phases constituting the composite ceramics (Fig. 1).

Ceramic samples of $Ce_{1-x-y}Gd_xM_yO_{2-\delta}$ (M = Mn and Co; $x = 0.10$ and 0.20; $y = 0.02-0.40$) were prepared by the standard ceramic route in order to study the effects of doping with the transition metal oxides on the transport properties of gadolinia-doped ceria. These samples were sintered in air at 1670 to 1800 K during 10–15 h. Additional information on $Ce(Gd,M)O_{2-\delta}$ can be found elsewhere [18,22–24].

Prior to further studies, all ceramic samples were annealed in air at 1170 K for 8 to 15 h with subsequent slow cooling, in order to obtain oxygen nonstoichiometry values as close as possible to the equilibrium at low temperatures.

Sample characterization was carried out by X-ray diffraction (XRD), scanning electron microscopy and energy dissipative spectroscopy (SEM/EDS), dilatometry, impedance spectroscopy and four-probe DC electrical conductivity measurements; the experimental procedures and equipment used for the characterization were reported elsewhere (Refs. [5,11,18–24]). The details on the measurements of steady-state oxygen permeation fluxes were also published earlier [5,11,21,22]. The permeation tests were carried out in the temperature range 1023–1223 K. For all data on oxygen permeability presented in this paper, the membrane feed-side oxygen partial pressure (p_2) was maintained at 21 kPa (atmospheric air).

In this article, the oxygen permeation processes are discussed using the quantities permeation flux density j (mol s^{-1} cm^{-2}) and specific oxygen permeability $J(O_2)$ (mol s^{-1} cm^{-1}) interrelated as [25]

$$J(O_2) = j \times d \times \left[\ln \frac{p_2}{p_1}\right]^{-1} \quad (1)$$

where d is the membrane thickness, and p_1 is the oxygen partial pressure at the membrane permeate side. The quantity $J(O_2)$ is suitable to identify a limiting effect of surface exchange rate on the oxygen permeation by analyzing dependence of the permeation flux on membrane thickness. This quantity is, by definition, proportional to $j \times d$, and should not depend on thickness when surface limitations are negligible. In this situation, $J(O_2)$ is proportional to

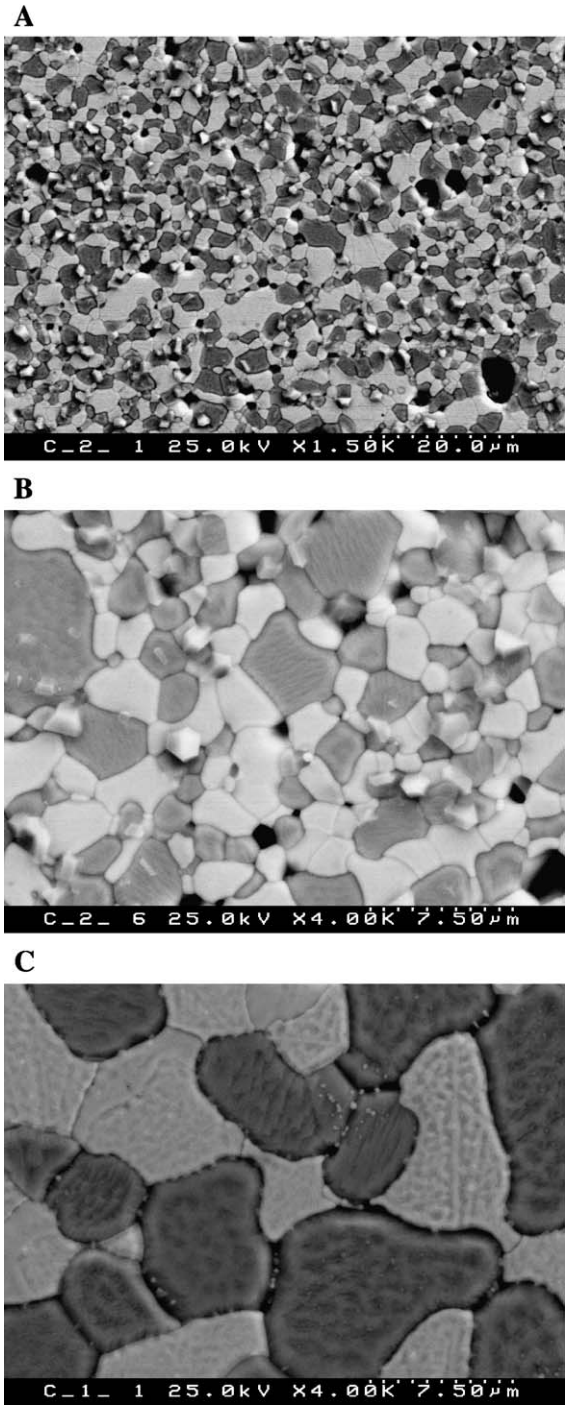

Fig. 1. Backscatter electron images of the composite ceramics: LSFC/CGO-1 (A and B) and LSFC/CGO-2 (C).

the so-called ambipolar conductivity (σ_{amb}), averaged for a given oxygen partial pressure range:

$$J(O_2) = \frac{RT}{16F^2} \times \overline{\sigma_{amb}} = \frac{RT}{16F^2} \times \frac{\overline{\sigma_o \times \sigma_e}}{\sigma_o + \sigma_e} = \frac{RT}{16F^2} \times \overline{\sigma \times t_o(1 - t_o)} \quad (2)$$

where t_o is the oxygen ion transference number, and σ, σ_o and σ_e represent the total, oxygen ionic and electronic conductivities, respectively. Here, σ_e is the sum of the n-type and p-type contributions ($\sigma_e = \sigma_n + \sigma_p$). When oxygen exchange influences the overall ion transfer, the value of $J(O_2)$ should increase with membrane thickness at a given oxygen chemical potential gradient owing to a decreasing role of the surface exchange.

The values of the activation energy (E_a) for both electronic and ionic conductivities, reported in this paper, were calculated from fits to the standard Arrhenius model:

$$\sigma = \frac{A_0}{T} \times \exp\left(-\frac{E_a}{RT}\right) \quad (3)$$

where A_0 is the pre-exponential factor.

Table 2
XRD results and thermal expansion coefficients of the ceramic materials

Material	Phase composition[a]	Unit cell parameters ($\pm$ 0.0001 nm)[b]	$\bar{\alpha} \times 10^6$, K^{-1} (300–1050 K)
CGO20	F	$a_F = 0.5425$ nm	11.5 ± 0.1
CGPO	F	$a_F = 0.5423$ nm	11.0 ± 0.1
LSFC	P	$a_P = 0.5481$ nm, $\alpha = 60.56^0$	12.9 ± 0.3
LSM	P	$a_P = 0.5468$ nm, $\alpha = 60.42^0$	11.70 ± 0.07
LSFC/CGO-1	F + P	$a_F = 0.5446$ nm; $a_P = 0.5465$ nm, $\alpha = 60.49^0$	12.6 ± 0.3
LSFC/CGO-2	F + P	$a_F = 0.5451$ nm; $a_P = 0.5468$ nm, $\alpha = 60.49^0$	–
LSFC/CGPO	F + P	$a_F = 0.5445$ nm; $a_P = 0.5471$ nm, $\alpha = 60.53^0$	12.7 ± 0.2
LSM/CGO	F + P	$a_F = 0.5446$ nm; $a_P = 0.5470$ nm, $\alpha = 60.49^0$	11.7 ± 0.1
$Ce_{0.80}Gd_{0.10}Co_{0.10}O_{2-\delta}$	F	$a_F = 0.5417$ nm	11.9 ± 0.4

[a] "F" and "P" correspond to the fluorite and perovskite phases, respectively.
[b] a_F is the parameter of the cubic fluorite-type lattice; a_P and α are the parameters of rhombohedrally distorted perovskite unit cell.

3. Results and discussion

3.1. Properties of $La_{0.8}Sr_{0.2}Fe_{0.8}Co_{0.2}O_{3-\delta}$

XRD analysis of LSFC ceramics revealed a single rhombohedrally distorted perovskite phase; the unit cell parameters are presented in Table 2. The phase purity of the ceramics was verified by SEM/EDS. The microstructure of LSFC ceramics (Fig. 2), consisting of relatively large grains (2–10 μm), appears clean from any second phases. The smaller grains of about 1–2 μm observed after thermal treatment at the surface of polished samples (Fig. 2A) have the same chemical composition as the larger ones.

Table 2 lists the values of the thermal expansion coefficient (TEC) of the different materials, calculated from dilatometric data (Fig. 3) and averaged in the temperature range 300–1050 K. The TEC of LSFC, $(12.9 \pm 0.3) \times 10^{-6}$ K^{-1}, is slightly higher than the TEC of 20% gadolinia-doped ceria ceramics, $(11.5 \pm 0.3) \times 10^{-6}$ K^{-1}. Such a difference, of about 12%, is within the limits acceptable to the materials compatibility (15–20%). From the viewpoint of thermal expansion, the compatibility of doped ceria and lanthanum–strontium manganite is significantly better with the difference in TEC values not exceeding 2% (see Table 2).

One should note that the average TECs of LSFC and CGO20 obtained in this work are slightly lower with respect to the literature data [26–28]. The thermal expansion coefficient of $Ce_{0.8}Gd_{0.2}O_{2-\delta}$ averaged at 300–1270 K was reported to be 12.5×10^{-6} K^{-1} [26], while the corresponding value for $La_{0.8}Sr_{0.2}Fe_{0.8}Co_{0.2}O_{3-\delta}$ was found equal to 14.8×10^{-6} K^{-1} [27] and 15.4×10^{-6} K^{-1} [28]. Along with experimental uncertainty and possible effects of ceramic microstructure on thermal expansion, this difference is due to the narrower temperature range used in the present work. Indeed, heating of LSFC ceramics up to 1120–1170 K

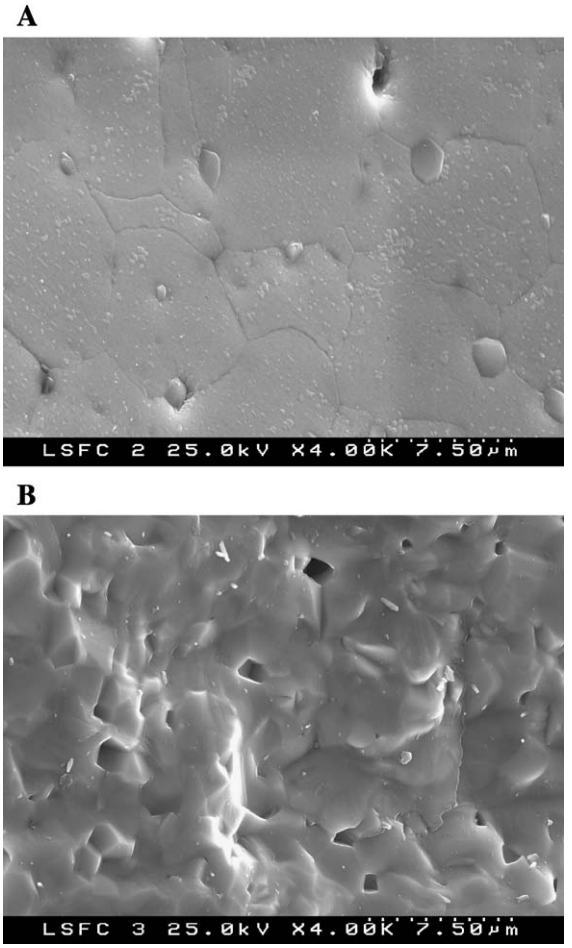

Fig. 2. SEM micrographs of LSFC ceramics: (A) after polishing and thermal treatment at 1470 K; (B) fractured sample.

resulted in a considerable nonlinearity of the dilatometric curves and a drastic increase of the expansion, associated with oxygen losses from the lattice when temperature increases. Again, such a feature suggests a limited compatibility of CGO20 and LSFC if used in high-temperature electrochemical devices.

The total conductivity of LSFC ceramics in air (Fig. 4), predominantly p-type electronic, is sufficiently close to the literature results [27,28]. The estimated apparent activation energy for the total conductivity is 12.2 ± 0.2 kJ/mol (Table 3), also in good agreement with the literature (13.5 kJ/mol [28]). The conductivity of $La_{0.8}Sr_{0.2}Fe_{0.8}Co_{0.2}O_{3-\delta}$ is slightly lower than that of $La_{0.7}Sr_{0.3}MnO_{3-\delta}$ (Fig. 4). However, at temperatures above 800 K, this difference is insignificant and may not affect the performance of composites consisting of the perovskite phases and CGO.

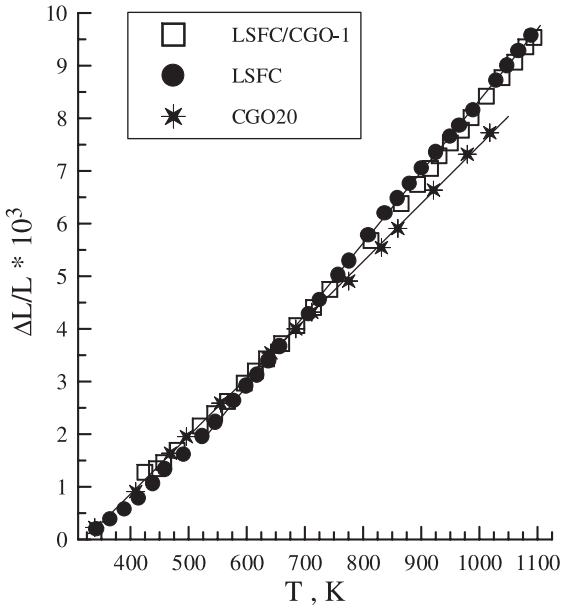

Fig. 3. Dilatometric curves of the studied ceramic materials in atmospheric air.

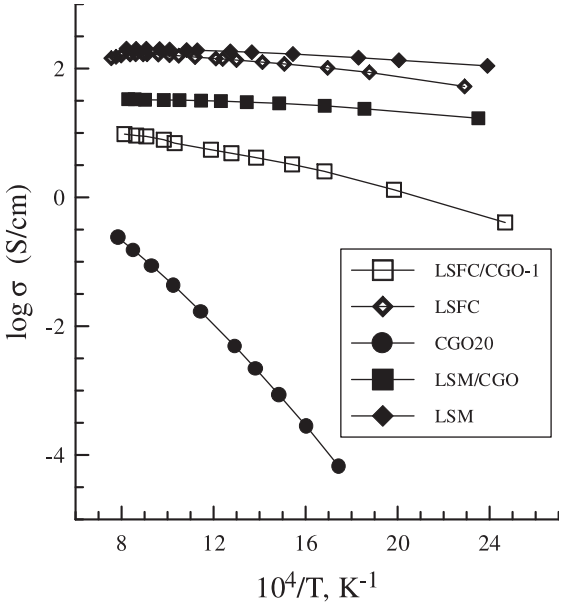

Fig. 4. Temperature dependence of the total electrical conductivity in air.

Table 3
Effective activation energy for the total conductivity of the ceramic materials in air

Abbreviation	T, K	E_a, kJ/mol	$\ln(A_0)$, S K/cm
LSFC/CGO-1	310–1230	21.5 ± 0.5	11.5 ± 0.1
LSFC	430–1100	12.2 ± 0.3	13.47 ± 0.05
LSM/CGO	360–1210	9.26 ± 0.09	11.52 ± 0.01
LSM	430–960	9.0 ± 0.3	13.23 ± 0.05

Fig. 5A shows the oxygen permeation fluxes through two LSFC membranes with different thickness as functions of the oxygen pressure gradient and temperature; the corresponding values of specific oxygen permeability are presented in Fig. 5B. Whilst oxygen fluxes increase with decreasing membrane thickness, the $J(O_2)$ values are independent of the thickness within the limits of experimental error. Such a behavior is in agreement with the integral form of Wagner law and unambiguously indicates that the oxygen transport is limited by the bulk ambipolar conductivity. This makes it possible to calculate the partial ionic conductivity of $La_{0.8}Sr_{0.2}Fe_{0.8}Co_{0.2}O_{3-\delta}$ from the permeation and total conductivity data (Eq. (2)). Continuing the comparison of LSFC and LSM phases, one can mention that oxygen permeability of the lanthanum–strontium ferrite–cobaltite is more than 200 times higher than that of lanthanum–strontium manganite [18]. Respectively, and in contrast to the LSM/CGO composites, ionic transport in LSFC/CGO composite ceramics might occur not only in the CGO phase, but also through LSFC phase.

Detailed data on physicochemical and transport properties of $Ce_{0.8}Gd_{0.2}O_{2-\delta}$ and $Ce_{0.80}Gd_{0.18}Pr_{0.02}O_{2-\delta}$, the second constituents in LSFC/CGO and LSFC/CGPO composites, were published elsewhere [18–21] and are not included in this paper.

3.2. Characterization of the composite ceramics

XRD data on LSFC/CGO and LSFC/CGPO composites confirmed the coexistence of two phases, with the fluorite- and perovskite-type structure. The lattice parameters (Table 2) show that the fluorite unit cell is larger in the composites than in pure ceria-based phases, while the opposite behavior is observed in the case of the perovskite. In addition, the observed CGO lattice expansion is greater in the composite LSFC/CGO-2 sintered at higher temperature and for a longer period of time. A similar behavior was observed for LSM/CGO composites [18].

The expansion of the ceria lattice is probably caused by incorporation of lanthanum and strontium cations, diffusing from the LSFC grains into the fluorite-type lattice [29]. The incorporation of the transition metal cations, Fe, Co and Mn, may also occur, but a contraction of the CGO unit cell should be observed in this case [18,22–24,30]. On the other hand, the diffusion of CGO cations to the LSFC phase is less probable. Numerous literature data (for instance, Ref. [31] and references therein) suggest a negligible dissolution of Ce^{4+} ions in the lattice of perovskite phases, where the A sublattice is mainly occupied by lanthanum and the B sites contain tran-

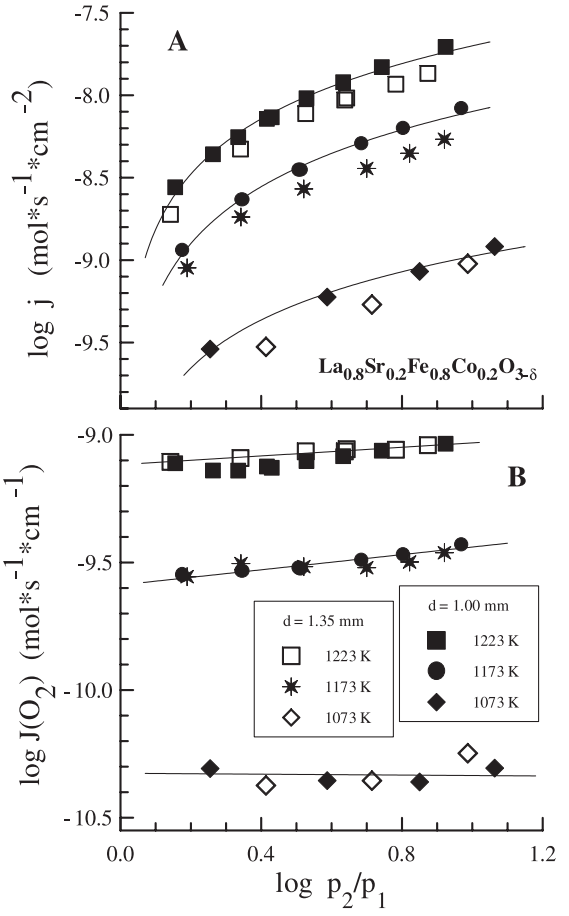

Fig. 5. Dependencies of the oxygen permeation fluxes (A) and specific oxygen permeability (B) of LSFC membranes on the oxygen partial pressure gradient. Solid lines are for visual guidance.

sition metal cations. Moreover, the thermodynamic stability of Gd-containing perovskites is lower than that of La-containing perovskite-type phases [31,32].

Diffusion of the cations constituting LSFC lattice into the ceria-based phase may lead to an imbalance between A-site and B-site cations in the perovskite structure, which can result in either A-site cation deficiency of the perovskite or segregation of iron and cobalt oxide phases. The smaller unit cell parameters of the perovskite phase in the composites with respect to pure LSFC (Table 2) indicate a formation of A-site cation vacancies. No segregation of the transition metal oxide phases at the grain boundaries was found by XRD and SEM/EDS analysis.

It should be mentioned that the interaction between $La_{0.8}Sr_{0.2}Fe_{0.8}Co_{0.2}O_{3-\delta}$- and ceria-based solid solutions may result not only in the dissolution of lanthanum and strontium in the fluorite-type lattice, but also in formation of $SrCeO_3$-based phases at the grain boundaries. As strontium cerate possesses relatively poor transport properties [33], segregation of $SrCeO_3$-based solid solutions might have a negative effect on ionic conduction in the composite materials. The SEM micrographs shown in Fig. 6 suggest the existence of a reaction product at the CGO/LSFC phase boundary; preliminary TEM studies confirmed that second perovskite-type phase with lattice parameter close to that of $SrCeO_3$ is often present. However, the composition of these boundaries was impossible to determine by EDS. Further TEM analysis is necessary in order to reveal if the formation of blocking $SrCeO_3$-based layers extensively occurs at the phase boundary between LSFC and ceria.

The percolation of both phases is clearly observed in back-scattered SEM micrographs (Fig. 1). Fig. 1B and C shows typical microstructures of LSFC/CGO-1 and LSFC/CGO-2 composites, respectively. Simple inspection of these micrographs shows an homogeneous phase distribution and that the grain size of both phases in the composites sintered at higher temperature and for longer time, LSFC/CGO-2, is about two to five times larger than in LSFC/CGO-1.

The observed linear behavior of the thermal expansion of the LSFC/CGO-1 composite (Fig. 3) can be seen as an indication of a reasonable degree of homogeneity in the phase distribution [34], in agreement with the SEM observations. With such homogeneous microstructure, the TEC of a composite usually

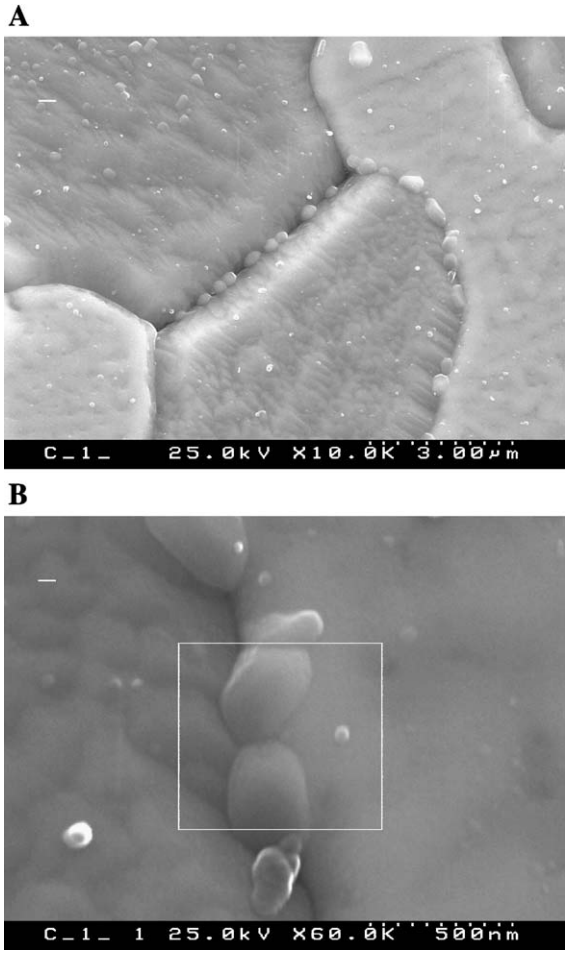

Fig. 6. SEM micrographs of LSFC/CGO-2 composite. The darker grains (A—center, B—left) correspond to LSFC phase.

results from the volume fraction and TEC of each individual component [35]. In fact, the estimated TEC value of the LSFC/CGO-1 composite ($(12.6 \pm 0.3) \times 10^{-6}$ K^{-1}) is within the limits of the TEC of both components.

Fig. 4 shows that the total conductivity of the composite ceramics is determined by the percolated phase having the highest conductivity, $La_{0.8}Sr_{0.2}Fe_{0.8}Co_{0.2}O_{3-\delta}$. Nevertheless, when comparing data on LSCF/CGO with LSM/CGO composites, one can note that, although the total conductivity of LSFC in air is close to that of LSM, the conductivity of LSFC/CGO ceramics is considerably lower with respect to LSM/CGO (Fig. 4). Also, while the activation energies for

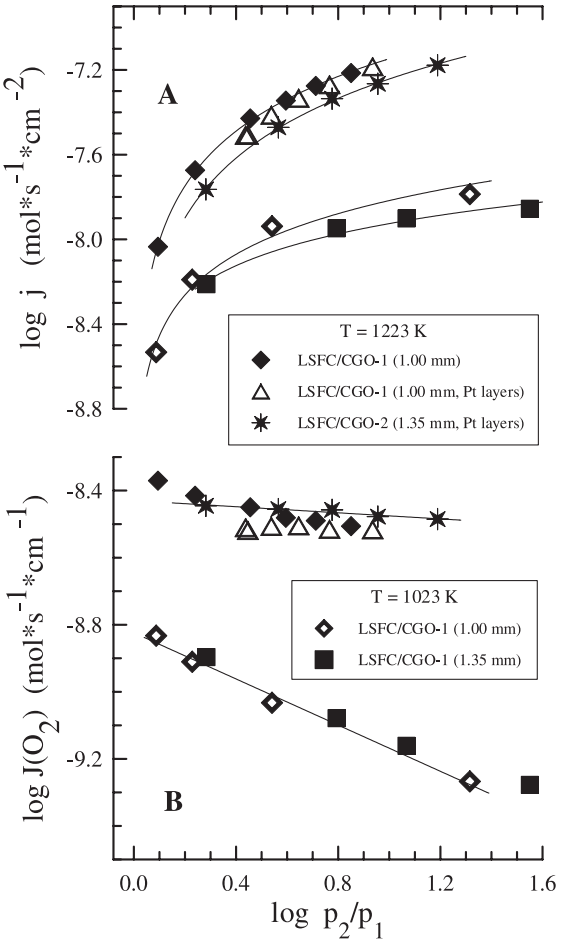

Fig. 7. Dependencies of the oxygen permeation fluxes (A) and specific oxygen permeability (B) of LSFC/CGO membranes on the oxygen partial pressure gradient. Solid lines are for visual guidance only.

the electronic conduction in LSM and LSM/CGO are similar, the E_a value for LSFC/CGO is almost two times higher than that of LSFC (Table 3). This behavior might be associated with grain boundary effects resulting from sintering of the LSFC/CGO ceramics at higher temperatures with respect to pure LSFC, which may lead to a phase segregation at LSFC grain boundaries in the composite. Traces of possible phase segregation at the boundaries of $La_{0.8}Sr_{0.2}Fe_{0.8}Co_{0.2}O_{3-\delta}$ grains were observed by SEM (Fig. 6A); EDS indicated a possible enrichment of LSFC grain boundaries with strontium. A grain-boundary blocking effect on the p-type electronic conduction in (La,Sr)$(Co,Fe)O_{3-\delta}$ ceramics has been earlier reported by Garcia-Belmonte et al. [36], who explained it in terms of double Schottky barriers.

3.3. Ionic conductivity

Selected results on oxygen permeation through LSFC/CGO membranes are given in Fig. 7. Within the reproducibility error, the specific oxygen permeability of the composite was independent of membrane thickness. Therefore, as for $La_{0.8}Sr_{0.2}Fe_{0.8}Co_{0.2}O_{3-\delta}$ ceramics, the limiting factor of the permeation is the bulk ambipolar conductivity. Note, however, that the reproducibility of the permeation fluxes through LSFC/CGO composites was considerably worse than for pure LSFC due to the presence of two phases and more complex transport mechanism. A LSFC/CGO membrane with porous platinum layers on both surfaces was tested in order to check for possible oxygen surface exchange limitations to the permeation. In many cases when the permeation-limiting role of the surface exchange is significant, the deposition of a catalytically active Pt layer onto the membrane surface leads to a greater oxygen permeability (for example, Refs. [37,38]). For the LSFC/CGO ceramics, the influence of applying such layers is negligible (Fig. 7).

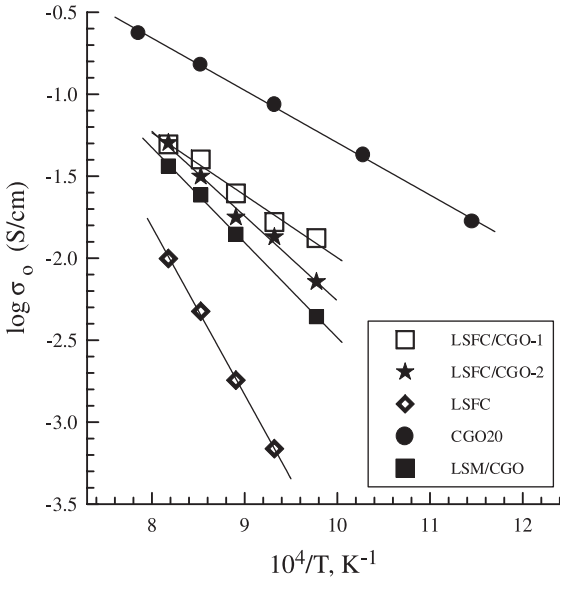

Fig. 8. Temperature dependence of the oxygen ionic conductivity of the ceramic materials under study.

Table 4
Effective activation energy for the oxygen ionic conductivity of the ceramic materials, calculated from the oxygen permeation and total conductivity data

Abbreviation	T, K	E_a, kJ/mol	$\ln(A_0)$, S K/cm
LSFC/CGO-1	1023–1223	82 ± 14	12 ± 1
LSFC/CGO-2	1023–1223	108 ± 14	15 ± 1
LSFC	1073–1223	206 ± 9	23 ± 1
LSM/CGO	1073–1223	106 ± 7	13.9 ± 0.7

The fact that the permeation fluxes through LSFC and LSFC/CGO membranes are predominantly limited by the bulk oxygen transport makes it possible to calculate the ion transference numbers and ionic conductivity from the data on oxygen permeability and total conductivity (see Eq. (2)):

$$\overline{\sigma_{amb}} = 4Fd \times \left(\frac{\partial j}{\partial E}\right)_{E\to 0} \quad (4)$$

$$t_o = \frac{1}{2} - \frac{1}{2}\sqrt{1 - 4\frac{\overline{\sigma_{amb}}}{\sigma}} \quad (5)$$

where E is the Nernst voltage:

$$E = \frac{RT}{4F} \times \ln\left(\frac{p_2}{p_1}\right) \quad (6)$$

For these calculations, only the permeation data corresponding to the permeate-side oxygen pressures in the range from approximately 5 to 21 kPa were used. The values of ionic conductivity are presented in Fig. 8, and Table 4 lists the values of the activation energy for oxygen ionic transport.

Although $La_{0.8}Sr_{0.2}Fe_{0.8}Co_{0.2}O_{3-\delta}$ exhibits considerably faster ionic conduction with respect to $La_{0.7}Sr_{0.3}MnO_{3-\delta}$, the ionic conductivity of LSFC/CGO and LSM/CGO composites with similar volume fractions of gadolinia-doped ceria has comparable values. Moreover, the apparent activation energy for ionic transport in the composites is quite far from that in LSFC and close to CGO (Tables 4 and 5). Such behavior suggests that ionic conduction in the composites occurs mainly in the fluorite-type phase. It can also be seen that composites processed under more extreme sintering conditions, LSFC/CGO-2, have a lower ionic conductivity (Fig. 8). The cation interdiffusion and phase segregation at the LSFC/CGO grain boundaries are thus likely to decrease the ionic conductivity of CGO, especially near the boundaries, and to affect the total ionic conduction of the composite ceramics. This means that, possibly, the ionic transport is preferential along the interface boundaries of CGO and LSFC grains, while the conjugated transfer of electronic charge carriers takes place near the boundaries in the perovskite phase.

At temperatures below 1200 K, the oxygen ionic conductivity in the LSFC/CGO composites is higher than that in LSM/CGO, and this difference increases when temperature decreases. Such phenomenon cannot be attributed to the contribution of LSFC phase, which should increase with increasing temperature due to the higher activation energy for ionic transport in LSFC with respect to CGO (Tables 4 and 5). Probable reasons may refer to the smaller ion-blocking effect at the LSFC/CGO grain boundaries in comparison with LSM-containing composite and/or to a better stability of LSFC with respect to interaction with ceria. This may result, in particular, from the

Table 5
Transport properties[a] of CeO_2-based ceramic materials

Material	Ionic conductivity		p-type electronic conductivity	
	σ_o, S/cm 1123 K	E_a, kJ/mol	σ_p, S/cm 1123 K	E_a, kJ/mol
CGO20	0.11	72.9 ± 0.8 (723–1273 K)	4.2×10^{-4}	145 ± 8 (1073–1273 K)
CGPO	0.12	74.0 ± 0.8 (723–1273 K)	3.2×10^{-3}	125 ± 6 (873–1223 K)
$Ce_{0.90}Gd_{0.10}O_{2-\delta}$	8.1×10^{-2}	65 ± 2	–	–
$Ce_{0.80}Gd_{0.10}Co_{0.10}O_{2-\delta}$	2.3×10^{-2}	–	2.1×10^{-2}	–

[a] The data relate to the oxygen partial pressure gradient of 101/21 kPa, excepting $Ce_{0.80}Gd_{0.10}Co_{0.10}O_{2-\delta}$. For the latter, the estimates of the partial conductivities correspond to the approximate oxygen pressure gradient of 21/5 kPa.

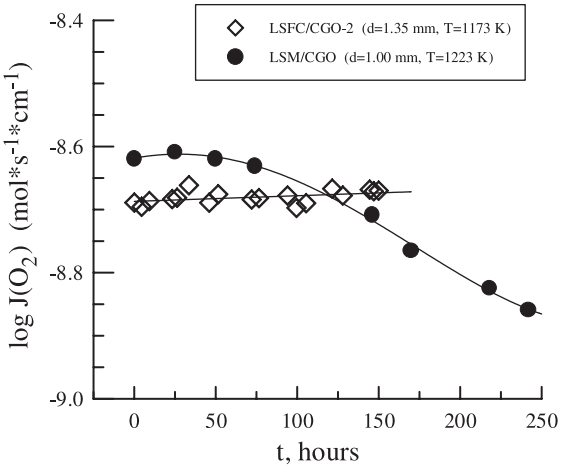

Fig. 9. Time dependencies of the oxygen permeability of LSFC/CGO and LSM/CGO membranes.

lower strontium concentration in $La_{0.8}Sr_{0.2}Fe_{0.8}Co_{0.2}O_{3-\delta}$ in comparison with $La_{0.7}Sr_{0.3}MnO_{3-\delta}$ and, hence, from the smaller amount of $SrCeO_3$-based phase formed at the grain boundaries of LSFC/CGO. The latter assumption is confirmed by the better stability of oxygen fluxes through LSFC/CGO ceramics. The long-term stability tests of the permeation fluxes through LSM/CGO membranes demonstrated their degradation, starting after annealing at 1173–1223 K for 70 to 100 h [18], whereas no significant degradation in behavior was observed for LSFC/CGO (Fig. 9).

3.4. The role of electronic conductivity of the ceria-based phase

In addition to the ionic transport in the CGO phase and conjugated electronic conduction in the LSFC phase, an important role in the oxygen transfer through composite ceramics can be played by the transport of both ionic and electronic charge carriers in CGO, resulting from the p-type conductivity of ceria. If the former mechanism may be associated with a greater resistance to the oxygen ion migration due to the relatively low ionic conductivity of LSFC and phase boundaries inside composite ceramics, the role of the latter would increase. The p-type electronic conduction in ceria can be increased by co-doping with variable-valence cations, such as Pr, Mn or Co. Values of the ionic and p-type electronic conductivities of CGO, CGPO and $Ce(Gd,M)O_{2-\delta}$ (M = Mn and Co) ceramics are listed in Table 5, while selected data on oxygen permeability are shown in Figs. 10 and 11.

Indeed, the oxygen permeation fluxes through LSCF-based composite membranes with Pr-doped CGO (LSCF/CGPO) are up to 25% higher than the fluxes through LSFC/CGO (Fig. 10). As the ionic conductivity values of $Ce_{0.8}Gd_{0.2}O_{2-\delta}$ and $Ce_{0.80}Gd_{0.18}Pr_{0.02}O_{2-\delta}$ ceramics are very close to each other [19,37], this behavior could be attributed to either p-type electronic conductivity of ceria-based phases or to the high electrocatalytic activity of Pr cations enhancing oxygen exchange. The oxygen exchange rate of $Ce_{0.80}Gd_{0.18}Pr_{0.02}O_{2-\delta}$ at 973 K and $p(O_2) = 101$ kPa is 50% higher than that of $Ce_{0.8}Gd_{0.2}O_{2-\delta}$ [39]. A similar conclusion can be drawn from the results on polarization resistance of Pt electrodes in contact with CGO20 and CGPO at 723–1073 K in air [40]. However, under the conditions studied in this work, the influence of the interfacial exchange on the oxygen permeability of composites was found negligible. The observed positive effect of Pr doping of the ceria phase should thus be related to the increase in the p-type

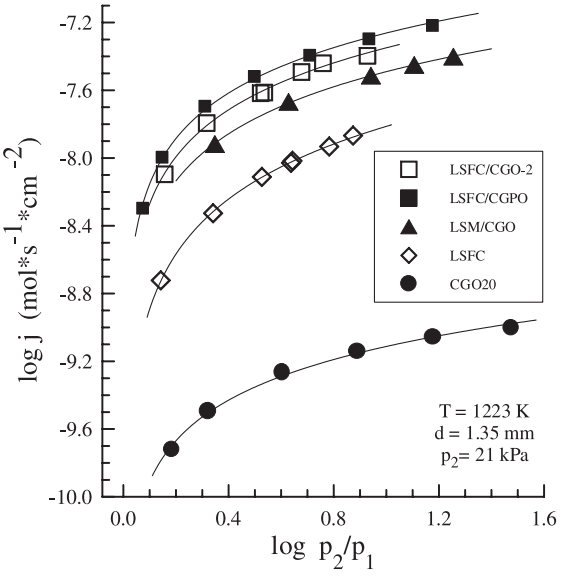

Fig. 10. Dependence of the oxygen permeation fluxes through ceria-based ceramic membranes on the oxygen partial pressure gradient. Solid lines are for visual guidance only.

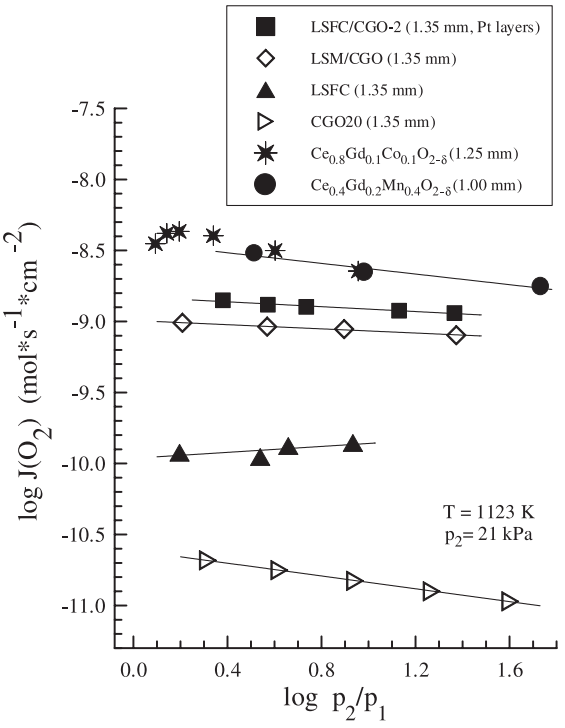

Fig. 11. Dependence of the specific oxygen permeability of selected materials under study on the oxygen partial pressure gradient. Solid lines are for visual guidance.

electronic conduction, increasing electrolytic permeability of the fluorite.

As for Pr-doped CGO, the permeation fluxes through $Ce(Gd,M)O_{2-\delta}$ (M = Mn or Co) membranes are also greater in comparison with the composites (Fig. 11). Although ionic conductivity of ceria decreases with additions of transition metal oxides [18,23], the p-type electronic conductivity in oxidizing conditions becomes much higher. Another important factor, providing the greater permeability of $Ce(Gd,M)O_{2-\delta}$, may refer to the smaller concentration of phase boundaries inside the ceramics in comparison with LSFC/CGO composites.

4. Conclusions

The average thermal expansion coefficient of perovskite-type mixed conductor $La_{0.8}Sr_{0.2}Fe_{0.8}Co_{0.2}O_{3-\delta}$ (LSFC) at 300–1050 K in air is equal to $(12.9 \pm 0.3) \times 10^{-6}$ K^{-1}, which is quite close to TEC of gadolinia-doped ceria (CGO) electrolytes and makes it possible to combine these materials in the dual-phase membranes. Oxygen permeability of both LSFC and composite LSFC/CGO ceramics at 970–1220 K is limited by the bulk ambipolar conductivity. Due to the relatively low ionic conductivity of LSFC and high activation energy for ionic transport in this phase (~ 200 kJ/mol), the contribution of the oxygen transfer through the perovskite phase to the total permeation fluxes through LSFC/CGO composite membranes was found considerably less in comparison with the ceria-based phase. As a particular result, the permeation fluxes through LSFC/CGO are comparable to those through LSM/CGO composites, containing similar volume fractions of doped ceria. Co-doping of ceria with variable-valence metal cations, such as Pr, Co or Mn, increases the p-type electronic conductivity in oxidizing conditions and thus leads to higher oxygen permeability. The oxygen ionic conduction in the composites, consisting of doped ceria and perovskite oxides, is strongly dependent of processing conditions, decreasing with interdiffusion of the phase components. Blocking oxygen ionic conduction is assumed to occur via forming low-conductive layers at the boundary of CGO grains due to diffusion of lanthanum and strontium cations into CGO phase. The stability of $La_{0.8}Sr_{0.2}Fe_{0.8}Co_{0.2}O_{3-\delta}$ in contact with gadolinia-doped ceria seems to be better than that of $La_{0.7}Sr_{0.3}MnO_{3-\delta}$ (LSM); the latter compound exhibits, however, a better compatibility with CGO from the viewpoint of thermal expansion.

Acknowledgements

This research was partially supported by the FCT (Praxis, Portugal), the Belarus Ministry of Education and Science, and the Belarus State University.

References

[1] H.J.M. Bouwmeester, A.J. Burgraaf, in: A.J. Burggraaf, L. Cot (Eds.), Fundamentals of Inorganic Membrane Science and Technology, Elsevier, Amsterdam, 1996, pp. 435–528.
[2] T.J. Mazanec, T.L. Cable, J.G. Frye, Solid State Ionics 53–56 (1992) 111.
[3] P.N. Dyer, R.E. Richards, S.L. Russek, D.M. Taylor, Solid State Ionics 134 (2000) 21.

[4] L. Qiu, T.H. Lee, L.-M. Liu, Y.L. Yang, A.J. Jacobson, Solid State Ionics 76 (1995) 321.
[5] V.V. Kharton, E.N. Naumovich, A.V. Nikolaev, J. Membr. Sci. 111 (1996) 149.
[6] H.L. Tuller, Solid State Ionics 94 (1997) 63.
[7] V.V. Vashook, M.A. Daroukh, H. Ullmann, Ionics 7 (2001) 59.
[8] E.W.J. Roemer, U. Nigge, T. Schulte, H.-D. Wiemhoefer, H.J.M. Bouwmeester, Solid State Ionics 140 (2001) 97.
[9] S. Pei, M.S. Kleefisch, T.P. Kobylinsky, J. Faber, C.A. Udovich, V. Zhang-McCoy, B. Dabrowski, U. Balachandran, R.L. Mieville, R.B. Poeppel, Catal. Lett. 30 (1995) 201.
[10] M. Schwartz, J.H. White, A.F. Sammells, Int. Patent Application PCT/WO/97/41060 (1996).
[11] V.V. Kharton, A.A. Yaremchenko, A.V. Kovalevsky, A.P. Viskup, E.N. Naumovich, P.F. Kerko, J. Membr. Sci. 163 (1999) 307.
[12] M.F. Carolan, P.N. Dyer, S.M. Fine, J.M. LaBar, R.M. Thorogood, US Patent 5,269,822 (1993).
[13] H.L. Tuller, Solid State Ionics 52 (1992) 135.
[14] V.V. Kharton, E.N. Naumovich, A.A. Vecher, J. Solid State Electrochem. 3 (1999) 61.
[15] C.S. Chen, A.J. Burggraaf, J. Appl. Electrochem. 29 (1999) 355.
[16] Y. Shen, A.V. Joshi, K. Krist, M. Liu, A.V. Virkar, US Patent 5,616,223 (1997).
[17] V.V. Kharton, E.N. Naumovich, A.A. Yaremchenko, F.M.B. Marques, J. Solid State Electrochem. 5 (2001) 160.
[18] V.V. Kharton, A.V. Kovalevsky, A.P. Viskup, F.M. Figueiredo, A.A. Yaremchenko, E.N. Naumovich, F.M.B. Marques, J. Electrochem. Soc. 147 (2000) 2814.
[19] V.V. Kharton, A.P. Viskup, F.M. Figueiredo, E.N. Naumovich, A.A. Yaremchenko, F.M.B. Marques, Electrochim. Acta 46 (2001) 2879.
[20] V.V. Kharton, F.M. Figueiredo, L. Navarro, E.N. Naumovich, A.V. Kovalevsky, A.A. Yaremchenko, A.P. Viskup, A. Carneiro, F.M.B. Marques, J.R. Frade, J. Mater. Sci. 36 (2001) 1105.
[21] F.M. Figueiredo, F.M.B. Marques, J.R. Frade, J. Eur. Ceram. Soc. 19 (1999) 807.
[22] E.N. Naumovich, V.V. Kharton, A.V. Kovalevsky, V.V. Samokhval, in: F. Poulsen, N. Bananos, S. Linderoth, M. Mogensen, B. Zachau-Christiansen (Eds.), Proc. 17th Riso Int. Symp. on Materials Science (Roskilde, Denmark, September 2–6), 1996, pp. 375–380.
[23] A.V. Kovalevsky, V.V. Kharton, E.N. Naumovich, Inorg. Mater. 32 (1996) 1230.
[24] E.N. Naumovich, V.V. Kharton, A.V. Kovalevsky, V.V. Samokhval, in: T.A. Ramanarayanan (Ed.), Ionic and Mixed Conducting Ceramics III, vol. PV97-24, The Electrochemical Society, Pennington, 1998, pp. 496–508.
[25] H.-H. Moebius, Extend. Abstr. 37th Meet. ISE, vol. 1, Int. Society of Electrochemistry, Vilnius, 1986, pp. 136–138.
[26] M. Mogensen, T. Lindegaard, U.R. Hansen, G. Mogensen, J. Electrochem. Soc. 141 (1994) 2122.
[27] A. Petric, P. Huang, F. Tietz, Solid State Ionics 135 (2000) 719.
[28] L.-W. Tai, M.M. Nasrallah, H.U. Anderson, D.M. Sparlin, S.R. Sehlin, Solid State Ionics 76 (1995) 259.
[29] H. Inaba, H. Tagawa, Solid State Ionics 83 (1996) 1.
[30] J.D. Sirman, D. Waller, J.A. Kilner, in: U. Stimming, S.C. Singhal, H. Tagawa, W. Lehnert (Eds.), SOFC-V, vol. PV97-40, The Electrochemical Society, Pennington, 1997, pp. 1159–1168.
[31] V.V. Kharton, A.A. Yaremchenko, E.N. Naumovich, J. Solid State Electrochem. 3 (1999) 303.
[32] H. Yokokawa, N. Sakai, T. Kawada, M. Dokiya, Solid State Ionics 52 (1992) 43.
[33] V.V. Kharton, A.A. Yaremchenko, E.N. Naumovich, F.M.B. Marques, J. Solid State Electrochem. 4 (2000) 243.
[34] F.M. Figueiredo, F.M.B. Marques, J.R. Frade, J. Electroceram. 7 (2001) 47.
[35] F.M. Figueiredo, F.M.B. Marques, J.R. Frade, Solid State Ionics 138 (2001) 173.
[36] G. Garcia-Belmonte, J. Bisquert, F. Fabregat, V. Kozhukharov, J.B. Carda, Solid State Ionics 107 (1998) 203.
[37] V.V. Kharton, V.N. Tikhonovich, L. Shuangbao, E.N. Naumovich, A.V. Kovalevsky, A.P. Viskup, I.A. Bashmakov, A.A. Yaremchenko, J. Electrochem. Soc. 145 (1998) 1363.
[38] V.V. Kharton, A.P. Viskup, A.V. Kovalevsky, F.M. Figueiredo, J.R. Jurado, A.A. Yaremchenko, E.N. Naumovich, J.R. Frade, J. Mater. Chem. 10 (2000) 1161.
[39] B.C.H. Steele, K.M. Mori, S. Uchino, Solid State Ionics 135 (2000) 445.
[40] V.V. Kharton, A.P. Viskup, F.M. Figueiredo, E.N. Naumovich, A.L. Shaulo, F.M.B. Marques, Mater. Lett. 53 (2002) 160.